A Triple-Emission Fluorescent Probe Reveals Distinctive Amyloid Fibrillar Polymorphism of Wild-Type α-Synuclein and Its Familial Parkinson's Disease Mutants

ARTICLE *in* BIOCHEMISTRY · AUGUST 2009

Impact Factor: 3.02 · DOI: 10.1021/bi9003843 · Source: PubMed

4 AUTHORS, INCLUDING:

María Soledad Celej
National University of Cordoba, Argentina
23 PUBLICATIONS **516** CITATIONS
SEE PROFILE

Wouter Caarls
Federal University of Rio de Janeiro
40 PUBLICATIONS **217** CITATIONS
SEE PROFILE

BIOCHEMISTRY
including biophysical chemistry & molecular biology
Article

Biochemistry **2009,** *48,* 7465–7472 7465
DOI: 10.1021/bi9003843

A Triple-Emission Fluorescent Probe Reveals Distinctive Amyloid Fibrillar Polymorphism of Wild-Type α-Synuclein and Its Familial Parkinson's Disease Mutants†

M. Soledad Celej,[‡,||] Wouter Caarls,[‡] Alexander P. Demchenko,[§] and Thomas M. Jovin*[,‡]

[‡]*Laboratory of Cellular Dynamics, Max Planck Institute for Biophysical Chemistry, am Fassberg 11, D37077 Göttingen, Germany, and* [§]*A. V. Palladin Institute of Biochemistry, 9 Leontovicha Strasse, 01030 Kiev, Ukraine.* [||]*Present address: Dto. de Química Biológica-CIQUIBIC, Facultad de Ciencias Químicas, Universidad Nacional de Córdoba, Haya de la Torre S/N, X5000HUA, Ciudad Universitaria, Córdoba, Argentina.*

Received March 6, 2009; Revised Manuscript Received May 11, 2009

ABSTRACT: Intracytoplasmic neuronal deposits containing amyloid fibrils of the 140-amino acid presynaptic protein α-synuclein (AS) are the hallmark of Parkinson's (PD) disease and related neurodegenerative disorders. Three point mutations (A53T, A30P, and E46K) are linked to early onset PD. Compared to the wild-type (WT) protein, the mutants aggregate faster in vitro, but their fibrillar products are quite similar. Using the extrinsic multiple-emission probe 4′-(diethylamino)-3-hydroxyflavone (FE), we demonstrate unique and distinct spectroscopic signatures for the amyloid fibrils formed by the WT and mutant AS, presumably indicative of subtle differences in supramolecular structure. The two well-separated emission bands of the FE probe originate from a proton transfer reaction in the excited state. The ratiometric response constitutes a sensitive, tunable reporter of microenvironmental properties such as polarity and hydrogen bonding. The very distinctive fluorescence spectra of the FE probe bound to the four AS variants reflect different tautomeric equilibria in the excited state and the existence of at least two different binding sites in the fibrils for the dye. Deconvolution of the two-dimensional excitation−emission spectra leads to estimations of different local dielectric constants and extents of hydration characteristic of the proteins. The sensitivity of such a simple external probe to conformational alterations induced by point mutations is unprecedented and provides new insight into key phenomena related to amyloid fibrils: plasticity, polymorphism, propagation of structural features, and structure−function relationships underlying toxicity.

Amyloidosis is pathognomonic of protein misfolding disorders characterized by the presence of intracellular or extracellular proteinaceous deposits. Mature amyloid fibrils have an unbranched rodlike morphology with a diameter of 7−13 nm and are usually formed from interwound protofilaments. The core structure is a stack of β-sheets in which the strands are perpendicular to the longitudinal axis of the fibril. This canonical cross-β structure is adopted by numerous proteins and peptides upon induction of aggregation in vitro (*1*, *2*). However, the fibrils originating from a given polypeptide can also demonstrate polymorphism. Ultrastructural variations, such as in the diameter, twist, pitch, and number of protofilaments, arise from fibril growth under altered conditions (*3*−*5*). In addition, molecular polymorphism, i.e., heterogeneity in three-dimensional (3D) conformation and orientation of the polypeptide chain, has been reported for some proteins (*2*−*7*). Of particular interest is the adaptability of the β-sheet network in amyloid fibrils to point mutations (*6*). Self-propagating polymorphs have important implications for species barriers, such as in prion biology and neurotoxicity. The same consideration applies to the elusive prefibrillar intermediates presumed to act as the primary toxic agents in disease (*2*). It follows that the elucidation of amyloid supramolecular assembly is an essential prerequisite for devising therapeutic agents and strategies.

The loss of dopaminergic neurons in the substantia nigra of the brainstem and the accumulation of intracellular inclusions (Lewy bodies) are the cardinal pathological features of Parkinson's disease (PD)[1] (*8*) and related disorders (*9*). The major component of these neuronal and glial cytoplasmatic inclusions is α-synuclein (AS), a presynaptic 140-amino acid protein whose normal function remains unclear (*9*, *10*). The native form of AS in solution is considered to be intrinsically disordered (*10*), although long-range domain interactions are presumed to stabilize an aggregation autoinhibited state (*11*). The perturbation of such tertiary interactions by single-point mutations may thus promote self-association and neurotoxicity (*12*). In fact, the three missense point mutations in the AS gene (A53T, A30P, and E46K) leading to early onset PD (*9*, *10*) share an increased tendency to fibrillize and/or form prefibrillar species in vitro (*10*).

The AS sequence comprises three functional domains: (i) the N-terminus (residues 1−60) with an amphipathic character

†This work was supported by the DFG Center for Molecular Physiology of the Brain (DFG CMPB), Cluster of Excellence 171 of the CMPB, in Göttingen, Germany, and the Max Planck Society (Toxic Protein Conformation project). M.S.C. was awarded a postdoctoral fellowship from the Alexander von Humboldt Foundation.

*To whom correspondence should be addressed. Telephone: +49-551-201-1381. Fax: +49-551-201-1467. E-mail: tjovin@gwdg.de.

[1]Abbreviations: PD, Parkinson's disease; AS, α-synuclein; NAC, non-amyloid component; WT, wild-type; NMR, nuclear magnetic resonance; AFM, atomic force microscopy; FE, 4′-diethylamino-3-hydroxyflavone; ESIPT, excited-state intramolecular proton transfer; N*, normal excited state; T*, tautomeric excited state; H-N*, hydrated form of the normal excited state; FWHW, full width at half-maximum.

Published on Web 07/08/2009

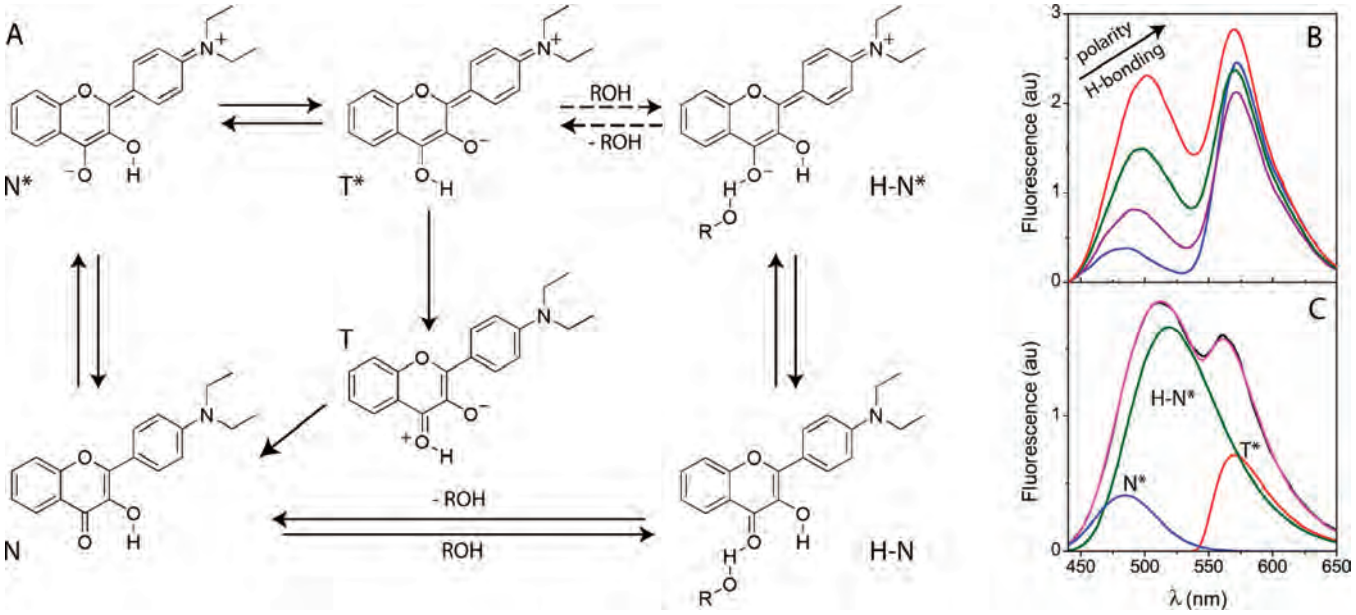

FIGURE 1: Spectroscopic attributes of the FE fluorescent probe. (A) Photophysical cycle. (B) Representative emission spectra of the FE dye in solvents with increasing polarities or degrees od H-bonding. (C) Spectral deconvolution into three bands corresponding to the emissive species shown in panel A. The experimental and fit fluorescence profiles are colored black and magenta, respectively.

typical of lipid binding domains, (ii) the hydrophobic aggregation-prone central NAC region (residues 61−95), and (iii) the highly acidic and proline-rich C-terminus (residues 96−140), which interacts with cationic ligands (*9*, *10*).

The monomers constituting wild-type (WT) AS fibrils are arranged in a parallel, in-register structure with a β-sheet-rich core region spanning residues 38−95 from which the two termini are excluded (*13*−*15*). By solid-state NMR, the N-terminus exhibits static disorder as of residue 22, whereas the C-terminus (residues 107−140) is unstructured and dynamic (*15*). Two apparent polymorphs of WT fibrils have been identified, varying in the extent and distribution of the β-structured core and distinct fibril morphologies (*15*). Two bundling states of WT AS fibrils differing in their protofilament interactions were also observed by cryoelectron microscopy (*16*), while changes in reaction conditions lead to morphologically distinguishable AS aggregates with differential binding capacity for amphiphilic fluorescent probes (*17*).

Fibrillar WT AS is distinguishable from familial mutants by EM (*18*) and AFM (*19*). According to immunochemical and protease digestion analysis, A30P fibrils have a conformation distinct from that of the WT that self-propagates in cross-seeded fibrillization (*20*). Solid-state NMR has also revealed significant differences between the WT and A30P mutant (*21*), as well as an extension of the β-sheet domain(s) of the A53T mutant to at least residues 38 and 100 (*22*). High-resolution structural data are unavailable.

A major aim of our investigations is to devise extrinsic and intrinsic fluorescence probes able to identify intermediates with distinct structural features during the early as well as the late phases of aggregation of AS. We recently reported two classes of compounds, *N*-arylaminonaphthalene sulfonates (*23*) and pyrene (*24*), that detect prefibrillar intermediates. In this study, we explored structural differences in amyloid fibrils formed by WT AS and the genetic mutants, employing 4′-(diethylamino)-3-hydroxyflavone (FE) as a sensitive multiple-emission fluorescent sensor of intermolecular interactions. As with other chromones exposed to aprotic media (*25*), FE undergoes a reversible excited-state intramolecular proton transfer [ESIPT (Figure 1A)] reaction, resulting in the formation of a tautomeric form (T*) emitting at longer wavelengths than the initial excited state (N*) (*26*). The species comprising the photophysical cycle differ in charge distribution, such that the fluorometric ratiometric response is highly sensitive to the polarity of the environment (*26*). Increased polarity greatly enhances the relative contribution of the N* band, which also experiences a bathochromic shift (Figure 1B) due to the stronger dipole moment of the N* state. In the framework of the continuous dielectric model that can be applied in the absence of intermolecular H-bonds (e.g., without water as the solvent), the dual-emission response of the FE dye spans a polarity range defined by a dielectric constant (ε) of ~2−47 (*26*).

An additional feature of this unique class of environmental probes is a third emissive species (H-N*) arising in protic media due to the formation of intermolecular H-bonds with solvent molecules (Figure 1A). The excitation spectrum of the H-N* form is red-shifted relative to the non-H-bonded species, and its emission band is located between those of N* and T*. It also undergoes ESIPT, albeit on a slower time scale, leading to a gradual transition to the T* form (*27*). This reaction does not generally contribute to the steady-state emission (*27*). Thus, the observed fluorescence spectra reflect the ground-state equilibrium between the N and H-N forms responsible for the initial distribution of excited-state species. Deconvolution of the resultant fluorescence spectrum into the three individual components (Figure 1C) provides the spectral locations and contributions of the emission bands, interpretable in terms of the local polarity and H-bonding experienced by the probe (*28*).

We compared the spectroscopic response of FE bound to amyloid fibrils formed from WT AS and the disease-related mutants. The dye exhibited distinctive multiple-emission profiles reflecting significant differences in the excited-state population and the existence of at least two binding sites. From the deconvolved spectra, we estimated apparent dielectric constants of the binding sites and evaluated the comparative hydration of the four fibrillar protein species. The results are discussed in terms of other available structural and spectroscopic data.

MATERIALS AND METHODS

Fluorescent Dye. The FE probe was kindly provided by A. S. Klymchenko (Louis Pasteur University, Strasbourg, France). The dye was synthesized, purified, and characterized according to the methods of ref *25*. Stock solutions were in ethanol, and working solutions were prepared by dilution into 25 mM Tris-HCl buffer (pH 7.2) and 100 mM NaCl immediately before use.

Fibril Preparation. AS variants were expressed in *Escherichia coli* and purified as described in ref *17*. Monomeric AS stock solutions were prepared in 25 mM Tris-HCl (pH 7.2) and 100 mM NaCl and centrifuged at 100000*g* before use to remove aggregates. Protein concentrations were determined by absorbance using an ε_{275} of 5600 M^{-1} cm^{-1} (*29*).

Fibril suspensions were obtained by incubating ~300 μM AS solutions in 25 mM Tris-HCl buffer (pH 6.2) and 100 mM NaCl, at 70 °C with constant shaking at 800 rpm in an Eppendorf Thermomixer comfort. Fibrils were purified by three consecutive cycles of centrifugation at 14000 rpm during 30 min in an Eppendorf MiniSpin plus centrifuge and resuspension in 25 mM Tris-HCl (pH 7.2) and 100 mM NaCl. Protein concentrations in monomeric units were determined by the absorbance of aliquots incubated in 6 M Gdm-HCl at 25 °C for 24 h.

Atomic Force Microscopy. Images were acquired on a Digital Instruments (Veeco) Multimode scanning probe microscope IIIa using a J-Scanner in air at a scan rate of 1 Hz with 512 lines per image. Imaging was performed in tapping mode with a silicon (nominal spring constant of 40 N/m) cantilever. An aliquot of the aggregated sample was diluted with water and spin-coated on a freshly cleaved mica surface.

Steady-State Fluorescence Measurements. Excitation and emission spectra were recorded with a Cary Eclipse spectrofluorimeter (Varian). Spectral slits were set at 5 nm. Additional built-in filters were used in both monochromatic channels (excitation at 335−620 nm, emission at 430−1100 nm) to reduce scatter. Spectra were recorded at 25 °C using a 3 mm path cuvette and corrected for wavelength-dependent excitation intensity and detection efficiency. Experiments were performed in quadruplicate at final concentrations of 10 μM protein and 1 μM probe.

Global Two-Dimensional Deconvolution. Emission spectra were deconvolved into three bands (N*, H-N*, and T*) using a global deconvolution over 11 excitation wavelengths in the wavenumber domain. Individual bands were approximated by a log-normal function accounting for four parameters: asymmetry, full width at half-maximum (FWHM), position, and height (*30*). All parameters, except the height, were held constant over all excitation wavelengths, and the N*:T* intensity ratio was constrained to a single value. The total number of parameters was 32.

Spectral deconvolution was performed using iterative nonlinear least-squares fitting implemented using the Levenberg−Marquardt technique provided by the MATLAB programming language. The parameters were initialized randomly in a suitable range and allowed to vary according the following constraints: 0.5 ≤ asymmetry ≤ 1, 500 ≤ fwhm ≤ 3500, and position of the N* band between 20000 and 20800 cm^{-1}. Deconvolution procedures and solvent calibrations are described in a separate communication (W. Caarls et al., manuscript submitted for publication).

RESULTS AND DISCUSSION

AS Fibrils Exhibit Distinctive Multiple-Emission Fluorescence Signatures upon Binding of the ESIPT Probe FE. The fibrillization of WT and mutant AS was induced by incubation of protein solutions at 70 °C with continuous shaking. The high temperature accelerates the aggregation, thereby facilitating the experimental procedures (*23*). Unbranched, polymorphic (straight as well as twisted) fibrils with heights of 6.3−8.3 nm (distinctive for each protein) were observed by AFM (Figure 2A). These materials were used in all experiments, with consistent results for independent fibrillar preparations of each protein.

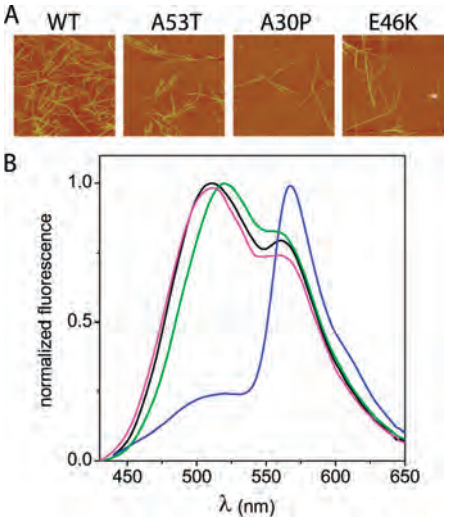

FIGURE 2: Morphology of AS fibrils and fluorescence signatures upon FE binding. (A) AFM images of AS fibrillized at 70 °C. Images are 3 μm × 3 μm. The measured heights (nanometers) were 7.7 ± 1.1 (WT), 7.3 ± 0.6 (A53T), 8.3. ± 0.9 (A30P), and 6.3 ± 0.6 (E46K) (n = 11). (B) Emission spectra of FE dye bound to WT (black), A53T (blue), A30P (green), and E46K (magenta) fibrils. λ_{exc} = 420 nm.

Upon interaction of the neutral, amphipathic FE dye with purified fibrils, two emission bands were observed, differing between the AS variants (Figure 2B). The fluorescence of FE in aqueous medium with or without the monomeric proteins was negligible, such that the signals were exclusively from the fibril-bound dye. The WT and E46K AS spectra were characterized by an intense N* band at ~510 nm and a minor T* band at ~560 nm. In contrast, the A53T mutant exhibited a prominent T* band at 567 nm, indicative of a nonpolar environment, while in the case of the A30P mutant, the short-emission band was red-shifted (~10 nm) compared to that of WT AS, reflecting a more polar and/or more hydrated microenvironment.

The features of the emission spectra indicated that FE molecules were screened from the solvent and located in a binding site(s) of low polarity with an apparent ε in the range of 2−47 (*26*). We conclude that the ESIPT probe senses differences in the local microenvironments in the WT and mutant forms of AS arising from distinctive supramolecular amyloid organizations.

Ground-State Heterogeneity of FE Bound to AS Fibrils. The breadth of the short-emission band in Figure 2B, and the small separation of the two peaks (~50 nm), usually 80−120 nm in reference systems (*26*), indicated a possible heterogeneity in the ground state. Accordingly, additional emission spectra were recorded for a number of excitation wavelengths. Figure 3A depicts the correlated excitation−emission spectra in 3D and the projected contour plots. Two discrete regions were apparent, differing significantly in relative height according to the identity of the AS protein.

Orthogonal sections through the correlated excitation−emission landscape (Figure 3B) indicated the presence of an additional emissive species. Red-edge excitation displaced the first

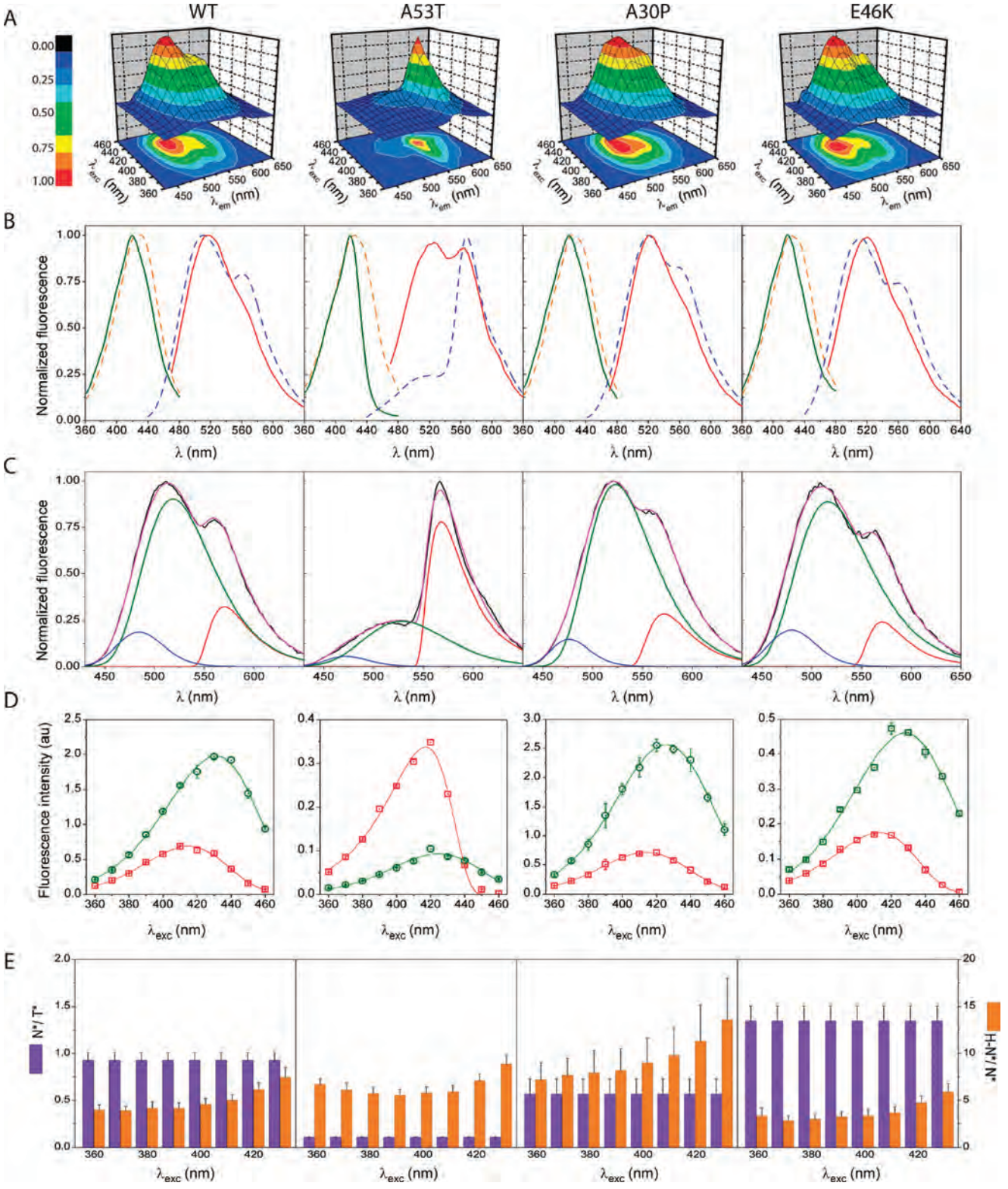

FIGURE 3: Ground-state heterogeneity and resolved component spectra of the FE dye bound to AS fibrils. (A) 3D representation and contour plots of correlated excitation−emission spectra. (B) Orthogonal sections through the 3D fluorescence landscape. The excitation spectra at λ_{em} values of 510 (orange) and 590 nm (green) and emission spectra at λ_{exc} values of 420 (blue) and 450 nm (red). (C) Deconvolved emission spectra. The experimental (black) and fit (purple) fluorescence profiles along with the individual components corresponding to the N* (blue), H-N* (green), and T* (red) forms. λ_{exc} = 420 nm. (D) Virtual excitation spectra obtained from the deconvolution for the N* or T* form (red squares) and the H-N* form (green circles). (E) Ratios of the integrated areas of the N* and T* bands (violet bars, left) and of the H-N* and N* bands (orange bars, right).

emission band to ~518 nm, and the T* band decreased in intensity. The latter effect was not attributable to reduction of solvent relaxation due to hindered motion (*31*). Instead, the findings suggested the existence of at least two bound species: (i) a non-H-bonded form with a dual emission (N* and T*) and (ii) a hydrated form selectively excited at the red edge and with a single emission band at ~518 nm (H-N*). A similar behavior has been reported for similar flavone derivatives bound to lipid vesicles (*28*).

The dependence of the excitation spectra on the emission wavelength provided further evidence for the postulated heterogeneity (Figure 3B). In the case of all four types of fibrils, the excitation spectra recorded at the red edge of the emission (~550 nm, the start of the T* band) were blue-shifted compared to those recorded for lower emission wavelengths. We interpret this shift as a preferential photoselection of (i) a nonhydrated ground-state form of the dye in a low-polarity, hydrophobic site, in coexistence with (ii) a hydrated form in a protic location allowing intermolecular H-bonding. On the basis of the findings of the previous investigation of fibrillar complexes with *N*-arylaminonaphthalene sulfonates (*23*), we tentatively assume that the two postulated sites are distinct, i.e., do not physically overlap. This issue is discussed further below.

Global Deconvolution Reveals Binding Site Polymorphism. The contributions of the three putative emissive species were determined by global deconvolution of the emission spectra (Figure 3A) into individual bands, approximated by log-normal functions as in the case of complexes with lipid membranes (*28*, *32*). We optimized the analyses by avoiding arbitrary, uncertain fixed parameters while constraining the asymmetry and FWHM of the three bands and the position of the N* band to physically plausible ranges. All parameters, with the exception of the intensities, were held constant for all excitation wavelengths. The N*/T* ratio was also considered to be invariant, inasmuch as the two bands presumably originate from the same ground state (Figure 1). The constraints were validated in control experiments in ethyl acetate, a solvent in which only the N* and T* bands arise (*26*). Representative experimental and fit emission spectra along with the deconvolved individual components are given in Figure 3C. The deconvolution procedure provided consistent results between replicates of all AS samples.

From the deconvolved spectra, virtual excitation spectra were constructed by plotting the peak emission intensities of the three bands for all excitation wavelengths (Figure 3D). Due to the constant N*/T* ratio, their excitation spectra were identical in shape, and only one curve is shown. The four replicates were rescaled and fit with a log-normal function to estimate peak positions. Although the two excitation bands overlapped strongly (Figure 3D), the H-N* band was red-shifted (424−431 nm) relative to the nonhydrated form (413−417 nm). The H-N form was preferentially excited toward the red edge (Figure 3D), giving rise to the observed changes in the emission spectra (Figure 3B).

We computed the areas under the individual emission bands and also employed their relative values as ratiometric quantities. The rationale was that area calculations compensate for fluctuations in correlated intensity−width estimations and are thus less subject to fitting errors than the peak intensities, thereby supplying more reliable estimations. The ratios of the band areas of N* and T* and of H-N* and N* are shown in Figure 3E. The first quantity is a sensitive indicator of binding site(s) polarity, and the second can be interpreted as a hydration factor (*28*).

The N*/T* intensity ratio is strongly correlated with the polarity of the medium (*33*), showing a linear dependence on the solvent polarity function described within a continuous dielectric model (*34*). It has served to estimate dielectric constants in lipid vesicles (*28*, *32*) and hydrophobic pockets in BSA (*35*). The N*/T* area ratios of Figure 3E indicate that the surrounding polarities of the dye bound to the four AS variants increased as follows: A53T < A30P < WT < E46K. On the basis of a calibration obtained with neat solvents (Figure 4), we estimated

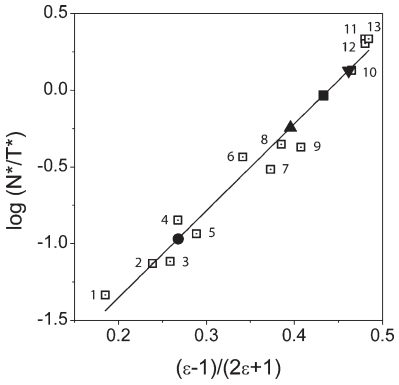

FIGURE 4: Solvent polarity scale for FE dye and estimation of polarity in fibrils. Logarithm of the N*:T* area ratio vs the polarity function $f(\varepsilon)$ for aprotic solvents (⊡). From 1 to 13: hexane, toluene, carbon disulfide, thiophene, di-*n*-butyl ether, anisole, bromobenzene, ethyl acetate, tetrahydrofuran, acetone, DMF, acetonitrile, and DMSO, respectively. The line is the best fit according to the correlation equation $\log(N^*/T^*) = -2.5 + 5.7f(\varepsilon)$ ($r = 0.96$). The corresponding values for WT (■), A53T (●), A30P (▲), and E46K (▼) fibrils are shown.

apparent ε values for the non-H-bonded binding site for FE dye on AS fibrils: WT AS, $\varepsilon \sim 11$, a value ranging between that of tetrahydrofuran and acetone; A53T mutant, $\varepsilon \sim 3$, a much lower value close to that of thiophene; A30P mutant, $\varepsilon \sim 7$, a value between that of ethyl acetate and that of tetrahydrofuran; and E46K mutant, $\varepsilon \sim 19$, corresponding to a more polar environment similar to acetone (Figure 4).

The familial mutants also exhibited different relative contributions from the H-bonded form of the dye in the second binding site (Figure 3E). Compared to the WT protein, this form was ~40 and 90% more prevalent in the A53T and A30P mutants, respectively (Figure 3E). Thus, the red shift in the first emission band of the A30P fibrils (Figure 2B) can be attributed to the increase in the contribution of the hydrated form (Figure 3E) rather than altered polarity (Figure 4). In contrast, the H-bonded form contribution was ~31% lower in the case of the E46K variant (Figure 3E).

The spectral deconvolution provided insight into structural features of the fibrils not apparent by simple inspection of the experimental spectra. The uncharged FE dye is amphipathic because of its polar CO and OH groups and the nonpolar moiety of the substituted chromone ring (Figure 1). Thus, the normal N* form coexists with a fraction of the H-N* form arising from interactions with OH or NH side groups of the protein or, more likely, with water of hydration. A quantitative determination of the fractional distribution of the probe between the two locations was not feasible because the respective quantum yields are unknown. Calibrations obtained in neat solvents are not applicable since nonemissive deactivation rates may be different in the protein environment.

The interpretations described above favor a distribution of the amphipathic probe between binding sites exhibiting a discrete number of H-bonding interactions rather than preferential binding to distinct fibrillar polymorphs. The notion of two binding microenvironments with different polarities was proposed in our previous study of *N*-arylaminonaphthalene sulfonate bound to WT AS fibrils (*23*). The time-resolved fluorescence measurements were compatible with a buried binding site excluded from water and an additional locus near the protein−solvent interface, where the dye experiences a more polar environment but restricted

motion (*23*). The existence of water-excluded cavities was also inferred in the study of pyrene-labeled AS variants, including the familial mutants (*24*), and from dissociation of AS fibrils exposed to high pressure (*36*). Void spaces arising from loose packing have been implicated as a factor contributing to the polymorphism of amyloid fibrils (*37*).

Structural Interpretations. We have shown above that FE exhibits distinctive emission signatures upon binding to amyloid fibrils formed of WT AS and the disease-related mutant proteins. Deconvolution of the emission spectra indicates that these differences arise from partitioning of the dye between at least two locations differing in polarity and in the propensity for intermolecular H-bonding.

It is noteworthy that the spectral changes and the resolved band components do not fully correlate with the nature of the particular mutated amino acid. The Ala to Thr substitution in the A53T mutant should lead to an increase in local polarity but a reduced hydrophobicity (*38*). Water molecules would be excluded, but it seems unlikely that such a small change would induce the prominent T* band indicative of a nonpolar environment (Figures 2B and 3). In view of the OH group of Thr, it may be involved in the relative increase in the contribution of the hydrated FE form (Figure 3E).

The A30P substitution should also reduce the surrounding hydrophobicity (*38*), an effect consistent with the estimated lower dielectric constant. However, in the WT fibrils, and presumably in the mutant forms as well, the region of residue 30 is disordered and excluded from the cross-β core (*15*), such that the Pro substitution would be solvent-exposed. Nonetheless, the considerable increase of the H-N* form (Figure 3E) cannot be attributed to a direct interaction of the probe with this residue since Pro lacks a proton on the amide group.

The mutation from an acidic to a basic residue in the E46K variant would lead to a change in net charge without modification of hydrophobicity. However, the increased polarity surrounding the non-H-bonded FE probe and the smaller contribution of the hydrated form (Figure 3E) are not likely due to specific electrostatic interactions with the positive charged lysine in view of the low polarity, the absence of net charge, and the small ground-state dipole moment of the FE molecule.

We have previously demonstrated by solid-state NMR that WT and A53T AS differ in fibrillar structure. The disease-related mutant exhibits an extended β-sheet core region spanning residues 38−100 (*22*). Thus, changes in secondary structure can be expected at sites well apart from the mutation site. On the basis of this result and the properties of the substituted amino acids discussed above, it appears likely that the FE probe "acts at a distance", i.e., sensing conformational perturbation(s) at binding sites remote from the locus of mutation.

Because of the lack of high-resolution structural models for AS fibrils, the molecular mechanism by which FE distinguishes between fibrils formed from molecules differing only by a single amino acid substitution is a matter of speculation. However, some correlations can be made on the basis of other reported structural and spectroscopic data.

AS fibrils are arranged in a parallel, in-register structure with a cross-β core spanning residues 38−95 (*13*−*15*). According to preliminary solid-state NMR data, the cross-β structure may consist of stacked three- to five-stranded β-sheet dimers with a water-shielded core region extending from at least residue 65 to residue 89 (H. Heise, A. Kumar, and M. Baldus, personal communication). In the schematic representation of the three-stranded

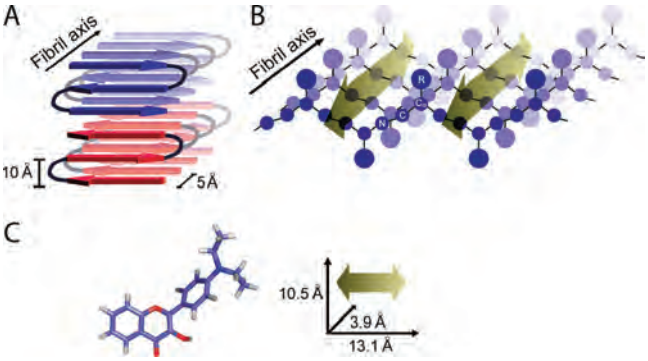

FIGURE 5: Proposed binding of FE dye to AS fibrils. (A) Parallel, in-register alignment of multiple β-strands in AS fibrils assuming an antiparallel orientation of three-stranded β-sheet monomers. (B) Schematic illustration of a β-sheet and tentative location of dye molecules (double headed arrow) in the binding channels based on ref *39*. Every strand corresponds to a different AS molecule. The backbone atoms and the side chain for one residue are indicated. (C) Stereochemical view and molecular dimensions of the FE dye obtained using ChemDraw and Chem3D: gray for H, red for O, blue for N, and light blue for C. The long axis of the double-headed arrow represents the longest axis of the FE molecule.

model (Figure 5A), successive incoming dimers are incorporated in the direction of fibril growth. Every layer of the parallel β-sheets can form channels formed by adjacent in-register side chains (Figure 5B). Such channels have been proposed as binding sites for thioflavin T, the probe most commonly used for detection of amyloid fibrils (*39*). Very recently, an alternative mechanism for thioflavin T binding to cross-strand ladders of Tyr residues in an antiparallel polypeptide was proposed (*40*). Since FE has dimensions similar to those of thioflavin T [tip-to-tail length of ~15 Å (Figure 5C)], we propose that it inserts into the β-sheet channels with the longest axis oriented parallel to that of the fibril (Figure 5B). A similar binding mechanism has been suggested for a series of organic dyes commonly used as polarity-sensitive probes (*23*) and cyanine derivatives (*41*).

The physical confinement conferred by the side chains along with partial shielding from bulk solvent molecules could lead to the observed spectroscopic properties. In the context of the proposed binding model, one site would be of low polarity and most probably embedded in the fibrils where the dye is protected from water molecules and surrounded by low-polarity residues. The other site would be closer to the protein−solvent interface where H-bonds with structural water molecules would form. We note that fibrillar conformations have been proposed for other proteins, e.g. β_2-microglobulin, differing in packing densities reflecting the presence of internal cavities and areas accessible to water (*42*). Invoking the concept of a hydrophobic-to-hydrophilic gradient extending from the core to the exposed surface of a typical globular protein (*43*), we propose that the different locations of the probe in a plane perpendicular to the fibril axis give rise to the different apparent dielectric constants, estimated from the N*:T* ratios, as well as the variable contribution from the hydrated H-N* form.

Although our fluorescence sensing approach cannot compete with crystallographic and NMR data in terms of atomic-scale resolution, it offers the advantage of very fine energy resolution of intermolecular interactions. The distinctive spectroscopic characteristics of the FE dye reveal differences in the amyloid organization of fibrils formed by WT AS and the disease-related variants. Further studies will contribute to a better understanding

of the plasticity of amyloid assemblies as they adapt to point mutations and their relationship to pathological conditions. We anticipate that both extrinsic and covalently attached dual (or in the present case triple)-emission probes will serve as useful tools not only for characterizing binding cavities in end-state fibrils but also for studying polymorphism and transmission of structural features in transient precursors arising in the overall aggregation pathway. In fact, in parallel experiments, certain covalent ESIPT conjugates of AS have demonstrated spectroscopic signatures (intensity, spectra) that appear to be specific for intermediate species, i.e., distinctive from those of the monomeric and terminal fibrillar forms of AS (D. Yuschenko et al., unpublished data). One can conclude that the ESIPT probes will render more systematic the selection of prospective inhibitors or reversers of aggregation.

ACKNOWLEDGMENT

We are very grateful to A. Pelah for the AFM measurements and A. Klymchenko for providing the FE dye and the fluorescence spectra in organic solvents. We acknowledge helpful discussions with R. Klement, D. Yushchenko, and E. Jares-Erijman.

SUPPORTING INFORMATION AVAILABLE

Results of global deconvolution of FE bound to WT (Figure S1), A53T (Figure S2), A30P (Figure S3) and E46K (Figure S4) AS fibrils. The asymmetry, FWHM, position and intensity of the individual FE emission bands for four fibrillar samples replicates and representative deconvolved emission spectra are shown. This material is available free of charge via the Internet at http://pubs.acs.org.

REFERENCES

1. Hamley, I. W. (2007) Peptide Fibrillization. *Angew. Chem., Int. Ed.,* 8128–8147.
2. Chiti, F., and Dobson, C. M. (2006) Protein misfolding, functional amyloid, and human disease. *Annu. Rev. Biochem. 75*, 333–366.
3. Kreplak, L., and Aebi, U. (2006) From the polymorphism of amyloid fibrils to their assembly mechanism and cytotoxicity. *Adv. Protein Chem. 73*, 217–233.
4. Chien, P., Weissman, J. S., and DePace, A. H. (2004) Emerging principles of conformation-based prion inheritance. *Annu. Rev. Biochem. 73*, 617–656.
5. Kodali, R., and Wetzel, R. (2007) Polymorphism in the intermediates and products of amyloid assembly. *Curr. Opin. Struct. Biol. 17*, 48–57.
6. Wetzel, R., Shivaprasad, S., and Williams, A. D. (2007) Plasticity of amyloid fibrils. *Biochemistry 46*, 1–10.
7. Novitskaya, V., Makarava, N., Bellon, A., Bocharova, O. V., Bronstein, I. B., Williamson, R. A., and Baskakov, I. V. (2006) Probing the conformation of the prion protein within a single amyloid fibril using a novel immunoconformational assay. *J. Biol. Chem. 281*, 15536–15545.
8. Bartels, A. L., and Leenders, K. L. (2008) Parkinson's disease: The syndrome, the pathogenesis and pathophysiology. *Cortex* (doi 10.1016/j.cortex.2008.11.010).
9. Shults, C. W. (2006) Lewy bodies. *Proc. Natl. Acad. Sci. U.S.A. 103*, 1661–1668.
10. Uversky, V. N. (2007) Neuropathology, biochemistry, and biophysics of α-synuclein aggregation. *J. Neurochem. 103*, 17–37.
11. Bertoncini, C. W., Jung, Y. S., Fernandez, C. O., Hoyer, W., Griesinger, C., Jovin, T. M., and Zweckstetter, M. (2005) Release of long-range tertiary interactions potentiates aggregation of natively unstructured α-synuclein. *Proc. Natl. Acad. Sci. U.S.A. 102*, 1430–1435.
12. Bertoncini, C. W., Fernandez, C. O., Griesinger, C., Jovin, T. M., and Zweckstetter, M. (2005) Familial mutants of α-synuclein with increased neurotoxicity have a destabilized conformation. *J. Biol. Chem. 280*, 30649–30652.
13. Serpell, L. C., Berriman, J., Jakes, R., Goedert, M., and Crowther, R. A. (2000) Fiber diffraction of synthetic α-synuclein filaments shows amyloid-like cross-β conformation. *Proc. Natl. Acad. Sci. U.S.A. 97*, 4897–4902.
14. Chen, M., Margittai, M., Chen, J., and Langen, R. (2007) Investigation of α-synuclein fibril structure by site-directed spin labeling. *J. Biol. Chem. 282*, 24970–24979.
15. Heise, H., Hoyer, W., Becker, S., Andronesi, O. C., Riedel, D., and Baldus, M. (2005) Molecular-level secondary structure, polymorphism, and dynamics of full-length α-synuclein fibrils studied by solid-state NMR. *Proc. Natl. Acad. Sci. U.S.A. 102*, 15871–15876.
16. Vilar, M., Chou, H. T., Luhrs, T., Maji, S. K., Riek-Loher, D., Verel, R., Manning, G., Stahlberg, H., and Riek, R. (2008) The fold of α-synuclein fibrils. *Proc. Natl. Acad. Sci. U.S.A. 105*, 8637–8642.
17. Hoyer, W., Antony, T., Cherny, D., Heim, G., Jovin, T. M., and Subramaniam, V. (2002) Dependence of α-synuclein aggregate morphology on solution conditions. *J. Mol. Biol. 322*, 383–393.
18. Giasson, B. I., Uryu, K., Trojanowski, J. Q., and Lee, V. M. (1999) Mutant and wild type human α-synucleins assemble into elongated filaments with distinct morphologies in vitro. *J. Biol. Chem. 274*, 7619–7622.
19. van Raaij, M. E., Segers-Nolten, I. M., and Subramaniam, V. (2006) Quantitative morphological analysis reveals ultrastructural diversity of amyloid fibrils from α-synuclein mutants. *Biophys. J. 91*, L96–L98.
20. Yonetani, M., Nonaka, T., Masuda, M., Inukai, Y., Oikawa, T., Hisanaga, S. I., and Hasegawa, M. (2009) Conversion of wild-type α-synuclein into mutant-type fibrils and its propagation in the presence of A30P mutant. *J. Biol. Chem. 284*, 7940–7950.
21. Kloepper, K. D., Woods, W. S., Winter, K. A., George, J. M., and Rienstra, C. M. (2006) Preparation of α-synuclein fibrils for solid-state NMR: Expression, purification, and incubation of wild-type and mutant forms. *Protein Expression Purif. 48*, 112–117.
22. Heise, H., Celej, M. S., Becker, S., Riedel, D., Pelah, A., Kumar, A., Jovin, T. M., and Baldus, M. (2008) Solid-state NMR reveals structural differences between fibrils of wild-type and disease-related A53T mutant α-synuclein. *J. Mol. Biol. 380*, 444–450.
23. Celej, M. S., Jares-Erijman, E. A., and Jovin, T. M. (2008) Fluorescent N-arylaminonaphthalene sulfonate probes for amyloid aggregation of α-synuclein. *Biophys. J. 94*, 4867–4879.
24. Thirunavukkuarasu, S., Jares-Erijman, E. A., and Jovin, T. M. (2008) Multiparametric fluorescence detection of early stages in the amyloid protein aggregation of pyrene-labeled α-synuclein. *J. Mol. Biol. 378*, 1064–1073.
25. Klymchenko, A. S., Pivovarenko, V. G., Ozturk, T., and Demchenko, A. P. (2003) Modulation of the solvent-dependent dual emission in 3-hydroxychromone by substituents. *New J. Chem. 27*, 1336–1343.
26. Klymchenko, A. S., and Demchenko, A. P. (2003) Multiparametric probing of intermolecular interactions with fluorescent dye exhibiting excited state intramolecular proton transfer. *Phys. Chem. Chem. Phys. 5*, 461–468.
27. Shynkar, V. V., Klymchenko, A. S., Piémont, E., Demchenko, A. P., and Mély, Y. (2004) Dynamics of intermolecular hydrogen bonds in the excited states of 4-dialkylamino-3-hydroxyflavones. On the pathway to an ideal fluorescent hydrogen bonding sensor. *J. Phys. Chem. A 108*, 8151–8159.
28. Klymchenko, A. S., Duportail, G., Demchenko, A. P., and Mely, Y. (2004) Bimodal distribution and fluorescence response of environment-sensitive probes in lipid bilayers. *Biophys. J. 86*, 2929–2941.
29. Weinreb, P. H., Zhen, W., Poon, A. W., Conway, K. A., and Lansbury, P. T., Jr. (1996) NACP, a protein implicated in Alzheimer's disease and learning, is natively unfolded. *Biochemistry 35*, 13709–13715.
30. Siano, D. B., and Metzler, D. E. (1969) Band shapes of the electronic spectra of complex molecules. *J. Chem. Phys. 51*, 1856–1861.
31. Demchenko, A. P. (2002) The red-edge effects: 30 years of exploration. *Luminescence 17*, 19–42.
32. Klymchenko, A. S., Mely, Y., Demchenko, A. P., and Duportail, G. (2004) Simultaneous probing of hydration and polarity of lipid bilayers with 3-hydroxyflavone fluorescent dyes. *Biochim. Biophys. Acta 1665*, 6–19.
33. Ercelen, S., Klymchenko, A. S., and Demchenko, A. P. (2002) Ultrasensitive fluorescent probe for the hydrophobic range of solvent polarities. *Anal. Chim. Acta 464*, 273–287.
34. Suppan, P., and Ghoneim, N. (1997) Solvatochromism , Royal Society of Chemistry, Cambridge, U.K.
35. Ercelen, S., Klymchenko, A. S., and Demchenko, A. P. (2003) Novel two-color fluorescence probe with extreme specificity to bovine serum albumin. *FEBS Lett. 538*, 25–28.
36. Foguel, D., Suarez, M. C., Ferrao-Gonzales, A. D., Porto, T. C., Palmieri, L., Einsiedler, C. M., Andrade, L. R., Lashuel, H. A.,

Lansbury, P. T., Kelly, J. W., and Silva, J. L. (2003) Dissociation of amyloid fibrils of α-synuclein and transthyretin by pressure reveals their reversible nature and the formation of water-excluded cavities. *Proc. Natl. Acad. Sci. U.S.A. 100*, 9831–9836.
37. Chatani, E., Kato, M., Kawai, T., Naiki, H., and Goto, Y. (2005) Main-chain dominated amyloid structures demonstrated by the effect of high pressure. *J. Mol. Biol. 352*, 941–951.
38. Li, J., Uversky, V. N., and Fink, A. L. (2001) Effect of familial Parkinson's disease point mutations A30P and A53T on the structural properties, aggregation, and fibrillation of human α-synuclein. *Biochemistry 40*, 11604–11613.
39. Krebs, M. R., Bromley, E. H., and Donald, A. M. (2005) The binding of thioflavin-T to amyloid fibrils: Localisation and implications. *J. Struct. Biol. 149*, 30–37.
40. Biancalana, M., Makabe, K., Koide, A., and Koide, S. (2009) Molecular mechanism of thioflavin-T binding to the surface of β-rich peptide self-assemblies. *J. Mol. Biol. 385*, 1052–1063.
41. Volkova, K. D., Kovalska, V. B., Balanda, A. O., Losytskyy, M. Y., Golub, A. G., Vermeij, R. J., Subramaniam, V., Tolmachev, O. I., and Yarmoluk, S. M. (2008) Specific fluorescent detection of fibrillar α-synuclein using mono- and trimethine cyanine dyes. *Bioorg. Med. Chem. 16*, 1452–1459.
42. Lee, Y. H., Chatani, E., Sasahara, K., Naiki, H., and Goto, Y. (2009) A comprehensive model for packing and hydration for amyloid fibrils of β2-microglobulin. *J. Biol. Chem. 284*, 2169–2175.
43. Park, H., and Jeon, Y. H. (2007) Cubic equation governing the outer-region dielectric constant of globular proteins. *Phys. Rev. E 75*, 021916.